Investigation of Thermoluminescent Properties of Synthetic (CVD) Diamond[1]

U. Biggeri, E. Borchi, M. Bruzzi, C. Leroy*, S. Sciortino

Department of Energetics, University of Florence, Florence, Italy

T. Bacci

Department of Mechanical Engineering, University of Florence, Florence, Italy

L. Ulivi, M. Zoppi

Institute of Quantum Electronics, CNR of Florence, Florence, Italy

C. Furetta

Department of Physics, University of Rome, Rome, Italy

items such as wear-resistant coatings, laser diode heat sinks and heat spreaders, optical windows, from the ultraviolet through the visible up to far infrared regions, for areospace and vacuum applications are already commercialized. Many other topics, such as developing microelectronic devices for high temperature, high power and radiation hard applications are still interesting fields of study and has generated significant research efforts. Fundamental limitations in the applications results from the polycrystalline structure of CVD diamond films and the presence of impurities and crystal defects.

The electronic properties of CVD diamond, such as high carrier mobility and high breakdown field, combined with the ability to produce thick layers of large area has open the possibility of its application to particle detection. CVD diamond with an excellent radiation hardness has been often presented as an alternative to silicon as detector of tracking devices in the adverse environment expected from the operation of the future Large Hadron Collider (LHC). Studies are presently carried on CVD diamond in view of its use as the active medium of sampling calorimeters[7,8] and particles high-precision trackers[9].

Diamond has a low atomic number (Z=6) and therefore is essentially a soft-tissue equivalent material (Z=7.4). Consequently, diamond is potentially an attractive material for applications in dosimetry, particularly in the medical field, in which the radiation absorption in the active material should be as close as possible to that of soft tissue. Moreover, it is stable, non toxic, radiation hard. Combined with its strength and availability in thin samples of very small volumes of precisely controlled dimensions, these features make it an attractive alternative to currently used TL dosimeters. The mechanism of growth allows to introduce precisely controlled impurities into diamond to give it high sensitivity. For clinical dosimetry, high accuracy of dose measurements is very important and if CVD diamond TL dosimeters can be produced of consistent quality, so that the dosimeters have identical response characteristics, then it will become possible to improve the accuracy of *in-vivo* clinical dosimetry. There are important reasons why it is necessary to seek such a development: recent improvements in radiotherapy treatment with multi-leaf collimators and stereo-tactic techniques permit precise shaping of treatment beams so that the dose distribution can be planned to conform the shape of the tumour. This reduces the irradiation of normal tissue in the vicinity of the tumour and allows higher doses to be delivered to the target volume. With the use of higher doses it becomes even more important to ensure that the prescribed dose is delivered within acceptable accuracy.

Preliminary results[10] on synthetic diamond stones, with boron and nitrogen impurities, have been recently reported, showing linearity up to a dose of 5 Gy, followed by a sub-linear region. The sensitivity was found to be 20% higher than that of LiF TLD-100. Moreover, similar TL response for gamma and beta radiation is observed.

Preliminary results on CVD diamond films have also been recently reported[11,12], leading to the conclusion that CVD diamond has a potential as a clinical dosimeter.

Some CVD diamond detectors have been found to be linear up to about one Gy and smoothly curved up to doses of 20 Gy and more. The linearity and reproducibility has been found at least, higher than for LiF. However, a limitation is observed by the fact that different batch of samples give different dose response.

A substantial step forward would consist in achieving a better control on the thermoluminescent response through a better understanding of the solid state properties, such as crystal defects or impurity concentration, that can affect the performance of CVD diamond dosimeters.

In the present paper thermoluminescent properties of CVD diamond are investigated. The thermoluminescence response of three CVD diamond samples to radiation exposure over a wide range of doses (from 60 mGy up to 3 Gy) was studied. This range of doses covers values found in therapy situations. The measurement of activation energies and frequency factors of the three CVD diamond samples was achieved by applying two standard methods. At first, a fit of the glow-curve intensity to the experimental glow-peaks was performed, assuming first order kinetics. Secondly, the peak-shape method was applied using three points from the isolated glow-curve peaks without assumption on the kinetics order. Moreover, a solid state characterization was performed on the samples in order to detect some relationship between the properties of the polycrystalline films and their different thermoluminescence response.

2. Thermoluminescence study of CVD diamond

The thermoluminescence properties of CVD diamond were investigated through three samples, hereafter referred to as AP071, AP076 and TP4R31. These measurements were performed at CERN with an Harshaw 3500 TLD reader. A linear rate of 2^{o}/s was applied from room temperature up to 400^{o} C. The irradiation doses were provided by a ^{90}Sr-^{90}Y β-source from 60 mGy to 3 Gy. Two measurements were also performed with a ^{241}Am γ-source (500 mGy and 3 Gy) to test the thermoluminescence response and linearity at higher doses. A one-hour annealing at 400^{o} C was performed between measurements in order of resetting the samples. A particular care was taken performing the measurements in a dark environment since a sensibility of the samples to light exposure was observed. Some measurements were taken repeatedly at the same dose level to ensure reproducibility.

The trapping paramaters were measured through two methods: a fit of the glow-curve intensities to isolated glow-peaks and a peak-shape analysis using three points from each isolated peak. The trapping parameters are: the activation energy (E), the frequency factor (s) and the order of kinetics (b).

3. Characterization of the samples

A characterization analysis of the samples was performed, following a standard working definition to separate diamond films from diamond-like carbon films[13]: a crystalline

morphology of the deposit discernible by electron microscopy, a single phase crystalline cubic diamond structure identified by diffraction techniques and a Raman spectrum typical of diamond.

At 300 K, the first-order Raman line of diamond[14] appears at 1332.5±0.5 cm^{-1} and has a halfwidth of 1.65±0.02 cm^{-1}. Raman spectra were measured at room temperature with the 514.5 nm radiation from an Ar^+ laser. The spectra were recorded with a Spex 1877 triple monochromator equipped with a liquid nitrogen cooled EG&G 1024×256 OMA4 CCD sensor. The spectra were measured in backscattering geometry and taken in the range 1100÷1700 cm^{-1}. In order to compare the quality of the films, with respect to bulk diamond a 1800 l/mm grating was employed with an entrance slit of 10 μm. The resolution achieved was about 0.5 cm^{-1}. The samples exhibited the characteristic line of diamond with no evidence of features due to graphite-like or amorphous carbon phases [13,15,16]. Table I shows the Raman shift and linewidths of the samples compared with the values of a natural Ia diamond[2]. The experimental spectra were fitted to a Lorentzian lineshape. Figure 1 shows the diamond line of sample AP071 compared with the diamond line of a film synthetized in Firenze with a DC plasma glow discharge method. We observe a broadening and a shift of the Raman line of the locally produced diamond with respect to the manufacturer's sample. It has been suggested that these features arise from an increase of compressive stress and scattering from defects in the film[18].

The high quality Raman spectra correlate with a highly faceted, large grained polycrystalline morphology. Figure 2 shows two SEM photograph of the growth and substrate side of sample AP071. On the substrate side of the film the grains are small, the grain size being of the order of a few microns. On the growth side of the films the grains are an order of magnitude larger and clear faceting is visible. This reflects a typical columnar grain structure, in which the grain size increases along the normal direction to the film.

Structural determination of the sample phases was accomplished by X-ray diffraction. Texturing was observed in all the samples. The ratio of the relative intensity was found to be different from sample to sample. Even for the same sample, the texturing at the growth side differs from that at the substrate side.

Figure 3 shows the diffraction pattern of sample AP071. We observe that the texturing at the substrate side is different from that at the growth side. At the substrate side two strong diffraction peaks (111) and (220) can be seen, while at the growth side the (220) peak is predominant.

At the substrate side (110) texturing and (111) texturing were found both in AP071 and AP076, while the substrate side of TP4R31 exhibited the diffraction pattern of α-SiC. At the growth side, strong (110) texturing was observed in all samples and it

[2]Type I diamonds contain nitrogen in one of four IR centres. Type IIb diamonds contain boron impurities in a substitutional form. Type IIa diamonds contain less than 20÷30 ppm of nitrogen and have the best optical properties and thermal conductivity[17].

has already been suggested that this is correlated with the columnar grain structure of the films[19].

A double Gaussian function was used for a least squares fit of the experimental diffraction peaks. From the values of the diffraction angle obtained from the fit, the lattice constant a can be calculated and the values obtained for the α_1 and α_2 lines can be averaged. Table II shows the values of the lattice constant, determined by the least squares fits and the relative standard deviations. Some lineshapes are shown in figure 4. We see that the α doublet is less resolved for sample AP076 than for sample AP071. This means that AP071 has a better film quality.

4. The fitting method

Single peaks were isolated for applying this method. A post-irradiation annealing was carried out in the reader itself to isolate the main peak and consisting of: an annealing at 400° C during one hour followed by an irradiation at a test dose of 60 mGy; a first readout using one step heating at 200° C for a period of 200 seconds to allow for the decay of the satellite structures at temperatures lower than that of the main peak; this is followed by a second readout performed with a linear heating rate of 2° C/s up to 400° C for a period of 200 seconds allowing to record the isolated main peak.

Assuming first order kinetics, the rate equation is given by[20]:

$$dn/dt = -pn \tag{1}$$

where n is the concentration (cm^{-3}) at the trap level, p is the probability per unit of time that a trapped carrier will escape from trap and is expressed as a function of temperature (T):

$$p = s\epsilon^{-E/kT} \tag{2}$$

where k, E and s are the Boltzmann's constant, the activation energy and the frequency factor, respectively. The glow-curve intensity (I) as a function of time (t) is then given by:

$$I(t) = n_0 s\epsilon^{-E/kT}\epsilon^{[-(s/q)\int_{T_0}^{T}\epsilon^{-E/kT}dT]} \tag{3}$$

n_0 is the number of trapped electrons at temperature T_0. q is the rate of the linear increase of temperature ($q = dT/dt$).

The thermoluminescent response of the three diamond samples as a function of dose (β and γ) is displayed in Figs. 5-7 which show that linearity is achieved over a wide range of radiation exposure. This linear increase indicates that all peaks grow at the same rate with radiation exposure. The shape and peak position of the glow-curve do not change with the dose. As an example, glow-curves corresponding to three different irradiation doses are shown in Fig. 8 for AP076, where the dotted lines and the solid lines represent the experimental data and the deconvolution peaks, respectively.

The values of activation energy and frequency factor were determined by fitting the glow-curve intensity (Eq. (3)) to the single peak of AP076 (Fig. 8), and the isolated main peaks of AP071 (Fig. 9) and TP4R31 (Fig. 10) for selected exposure doses. The values obtained are reported in Table III.

5. The peak-shape method

The shape of an isolated peak can be analyzed by means of three points from the glow-curve, without assumption on the kinetic order[21]. These are the peak temperature (T_M) at the maximum intensity and the temperatures T_1 and T_2 on either side of T_M corresponding to half-peak intensity. The following parameters can be defined: the full width of the peak at its half-height ($\omega = T_1 - T_2$), the high temperature half-width ($\delta = T_2 - T_M$) and the low temperature half-width ($\tau = T_M - T_1$). The activation energy is then given as:

$$E_\alpha = c_\alpha(kT_M^2/\alpha) - b_\alpha(2kT_M) \tag{4}$$

where $\alpha = \tau$, δ or ω. The constants, c_α and b_α for the three methods, assuming the frequency factor independent of temperature, are given by:

$$c_\tau = 1.51 + 3.0(\mu - 0.42) \quad \text{and} \quad b_\tau = 1.58 + 4.2(\mu - 0.42)$$

$$c_\delta = 0.976 + 7.3(\mu - 0.42) \quad \text{and} \quad b_\delta = 0.0$$

$$c_\omega = 2.52 + 10.2(\mu - 0.42) \quad \text{and} \quad b_\omega = 1.0$$

The constant $\mu = \delta/\omega$ is the symmetry factor. The values $\mu = 0.42$ and $\mu = 0.52$ correspond to a first order and second order kinetics, respectively.

The peak-shape method, based on three points from the glow-curve, heavily relies upon the accurate determination of the location of just three experimental points. Any inaccuracies, even slight, on these locations will produce erroneous values for the activation energy and consequently also on the frequency factor. Such inaccuracies can be due for instance to inefficient thermal cleaning of the lower temperature satellite peaks, yielding less reliable descending parts and width of the glow- curve. In order of minimizing possible inaccuracies on the location of the three reference points, the peak-shape method was applied on isolated curves as obtained from a fitting procedure which could be regarded merely in that approach as a smooth representation of the experimental peaks. According to that approach, no assumption was made on the kinetic order. The values of μ obtained from the points of the smoothed isolated glow-curves are given in Table IV and confirms that first order kinetics was faced for the three samples, supporting the assumption made in section 4. The values of the other trapping parameters found by applying this peak-shape method are also reported in Table IV. The values of the activation energy in Table IV are the weighted average of E_τ, E_ω, and E_δ. The frequency factors are calculated from:

$$s = (qE/kT_M^2)\epsilon^{E/kT_M}$$

6. DISCUSSION AND CONCLUSIONS

Thermoluminescent properties of three CVD diamond samples were investigated. A fitting procedure and a peak-shape analysis were applied on isolated peaks. In order to minimize possible inaccuracies on the location of the three reference points on which it is based on, the peak-shape method was applied on smoothed representation of the experimental isolated peaks. First order kinetic, assumed for the fitting method, was found as a result from the peak-shape method and confirmed the validity of the first order kinetic assumption made for the first method. Consistent measurements of the activation energies and frequency factors emerged from the two analysis. Both methods produced low values for the activation energy and the frequency factor. The frequency factor represents the number of times per second a bound electron interacts with the lattice phonons multiplied by a transition probability. The low values obtained for s and E indicate the relative facility for electrons to escape the traps of low depth that seem characterizing CVD diamond. These low values of the activation energy and frequency factor are consistent with earlier results obtained for natural diamond. Low values of activation energies for natural diamonds of type I and IIa have been reported [22] although without quoting any value for s.

The thermoluminescence response of the three CVD diamond samples exhibits linearity with radiation exposure over a wide range (from 60 mGy up to 3 Gy) which covers dose values found in therapy situations. The observed linear increase indicates that all peaks grow at the same rate with radiation exposure.

Moreover the present study suggests a relationship between the thermoluminescent response of the samples and their crystal quality. In fact, it has been observed that the Raman quality and the diffraction peak resolution was slightly better for the most sensitive sample (AP071) compared with the less sensitive one (AP076.) This assumption requires further investigation.

Acknowledgements

The authors are indebted to R.S. Sussmann from De Beers Diamond Research Laboratory for lending the diamond film specimens used in the present study. They also acknowledge the TIS division of CERN for making the equipment for thermoluminescence measurements available to them.

References

1. W. Zhu, B. R. Stoner, B. E. Williams and J. Glass, "Growth and Characterization of Diamond Films on Nondiamond Substrates for Electronic Applications," *Proc. IEEE* **79**, 5 (1991).

2. P. K. Bachmann and H. Lydtin, "High Rate Versus Low Rate Diamond CVD Methods," *Diamond and Diamond-Like Films and Coatings, NATO Advanced Study Institute on Diamond and Diamond-Like Films and Coatings*, (1990, Castelvecchio Pascoli, Italy) edited by R. E. Clausing, J. C. Angus, L. L. Horton and P. Koidl, Plenum Press, New York, 1991, p. 829.

3. P. K. Bachmann, "Microwave Plasma CVD and Related Techniques for Low Pressure Diamond Synthesis," *Thin Film Diamond*, edited by A. Lettington and J. W. Steeds, Chapman & Hall, London, 1994, p. 31.

4. G. Lu and L. K. Bigelow, "Material Properties of CVD diamond produced by the DC arc-jet," *Diamond Related Mater.* **1**, 134 (1992).

5. K. J. Gray, "Electromagnetic Window Properties of CVD Diamond," in *Proc. Conf. on Diamond Optics V, SPIE* **1759**, 203 (1992).

6. R. S. Sussmann, "Diafilm, A New Diamond Material for Optocs and Electronics," *Industrial Diamond Review*, **2**, 1 (1993).

7. R. J. Tesarek *et al.*, "First Beam Test Results of a Diamond-Tungsten Sampling Calorimeter," *Conference Proceedings, Vol. 46, 1st International Conference on Large Scale Applications and Radiation Hardness of Semiconductor Detectors*, (1993, Firenze, Italy) edited by A. Baldini and E. Focardi, SIF, Bologna, 1994.

8. R. J. Tesarek *et al.*, "Performance of a Diamond-Tungsten Sampling Calorimeter," *Nucl. Instr. and Meth. A* **349**, 96-105 (1994).

9. F. Borchelt *et al.*,"First Measurements with a Diamond Microstrip Detector," CERN PPE/94-113, to be published in *Nucl. Instr. and Meth. A*.

10. O. Avila and A. E. Buentil, "Diamond TL Response to Alpha, Beta and Gamma Radiation," *Radiation Protection Dosimetry* **58**, 61-63 (1995).

11. P. J. Hopwood and C. H. Jones, "Development of Synthetic Diamond as a Clinical Dosimeter," *Proc. of Diamond Conference*, (11-14th July 1993, Bristol, UK), published by De Beers Industrial Diamonds, 29.1-29.4 (1993).

12. P. J. Hopwood and C. H. Jones, "Development of the CVD Diamond as a Thermoluminescent Dosimeter for Radiotherapy," *Proc. of Diamond Conference*,

(11-13th July 1994, Reading, UK), published by De Beers Industrial Diamonds, 20.1-20.3 (1995).

13. P. K. Bachmann and D. U. Wiechert, "Characterization and Properties of Artificially Grown Diamond." *Diamond and Diamond-Like Films and Coatings, NATO Advanced Study Institute on Diamond and Diamond-Like Films and Coatings*, (1990, Castelvecchio Pascoli, Italy) edited by R. E. Clausing, J. C. Angus, L. L. Horton and P. Koidl, Plenum Press, New York, 1991, p. 677.

14. S. A. Solin and A. K. Ramdas, "Raman Spectrum of Diamond," *Phys. Rev. B* **1**, 1687 (1970).

15. R. E. Shroder, R. J. Nemanich and J. T. Glass, "Analysis of the Composite Structures in Diamond Thin Films by Raman Spectroscopy," *Phys. Rev. B* **41**, 3738 (1990).

16. W. A. Yarbrough and R. Messier, "Current Issues and Problems in the Chemical Vapor Deposition of Diamond." *Science* **247**, 688 (1990).

17. C. D. Clark, R. W. Ditchburn and H. B. Dyer, *Proc. Roy. Soc.* **A234**,363 (1956) (where a classification of diamonds can be found).

18. J. W. Ager III, D. K. Veirs and G. M. Rosenblatt, "Spatially Resolved Raman Studies of Diamond Films Grown by Chemical Vapour Deposition," *Phys. Rev. B* **43** 6491 (1991).

19. Shulai Zhao, "Characterization of the Electrical Properties of Polycristalline Diamond Films," The Ohio State University, 1994.

20. S.W.S. McKeever,"Thermoluminescence of solids." Cambridge University Press, Cambridge (1985).

21. R. Chen, *J. Appl. Phys.* **40** 570 (1969); R. Chen, *J. Electrochem. Soc.* **116**, 1254 (1969).

22. J. Nahum and A. Halperin, *J. Phys. Chem. Solids* **24**, 823 (1963).

Table captions

Table I: Raman shifts and linewidth of the samples compared with the measured values of a Ia diamond. Spectra were taken on the growth side of the films.
Table II: Lattice constants of the samples as coming out from the fitting procedure compared to the value of the lattice constant of natural diamond.
Table III: The values of the activation energy and frequency factor for the three CVD diamond samples, as obtained from the fitting method.
Table IV: The values of the parameters, activation energy and frequency factor as obtained from the application of the peak-shape method.

Figure captions

Fig. 1: Raman line of sample AP071 compared with the Raman line of a locally produced CVD film.

Fig. 2: SEM photographs. (a) Growth side of sample AP071, the magnification is 500. (b) Substrate side of sample AP071, The magnification is 3000.

Fig. 3: X-ray diffraction pattern of sample AP071: (a) Growth side; (b) Substrate side.

Fig. 4: Least squares fit of the α doublet of peak (220): (a) Sample AP071; (b) Sample AP076.

Fig. 5: The thermoluminescent response of AP071 (in arbitrary units) is shown as a function of the irradiation (β and γ) dose (in mGy).

Fig. 6: The thermoluminescent response of AP076 (in arbitrary units) is shown as a function of the irradiation (β and γ) dose (in mGy).

Fig. 7: The thermoluminescent response of TP4R31 (in arbitrary units) is shown as a function of the irradiation (β and γ) dose (in mGy).

Fig. 8 : Glow-curve lineshapes for AP076 (in arbitrary units) are shown for three doses (0.483 Gy, 0.967 Gy and 3.0 Gy). as a function of temperature (K).

Fig. 9 : A fit of the glow-curve intensity (Eq. (3)) to the AP071 isolated peak is shown for an irradiation dose of 60.5 mGy.

Fig. 10 : A fit of the glow-curve intensity (Eq. (3)) to the TP4R31 peak is shown for an irradiation dose of 3.0 Gy. as a superposition of fits to three deconvoluted peaks.

SAMPLE	RAMAN SHIFT	FWHM
	[cm^{-1}]	[cm^{-1}]
DIAMOND IA	1332.9	3.14
AP071	1331.7	3.6
AP076	1332.4	6.4
TP4R31	1332.2	3.7

Table I

SAMPLE	a [Å]	σ [Å]
NATURAL DIAMOND	3.57	
AP071	3.565	0.004
AP076	3.564	0.004
TP4R31	3.562	0.006

Table II

Sample	E (eV)	s ($10^7 s^{-1}$)
AP071	1.15 ± 0.20	70.0 ± 1.5
AP076	1.15 ± 0.20	70.0 ± 1.5
TP4R31	0.80 ± 0.15	0.058 ± 0.004

Table III

Sample	AP071	AP076	TP4R31
T_M (K)	581±2	582±2	573±2
T_1 (K)	547±2	548±2	527±2
T_2 (K)	605±2	607±2	608±2
μ	0.42±0.01	0.42±0.01	0.43±0.01
δ (K)	25±1	25±1	35±1
τ (K)	34±1	34±1	46±1
ω (K)	59±1	59±1	80±1
E_δ (eV)	1.13±0.07	1.13±0.06	0.86±0.04
E_τ (eV)	1.12±0.05	1.12±0.05	0.79±0.03
E_ω (eV)	1.13±0.06	1.13±0.06	0.82±0.04
E (eV)	1.13±0.06	1.13±0.06	0.83±0.04
s (10^7/s)	117±126	96±126	.14±0.08

Table IV

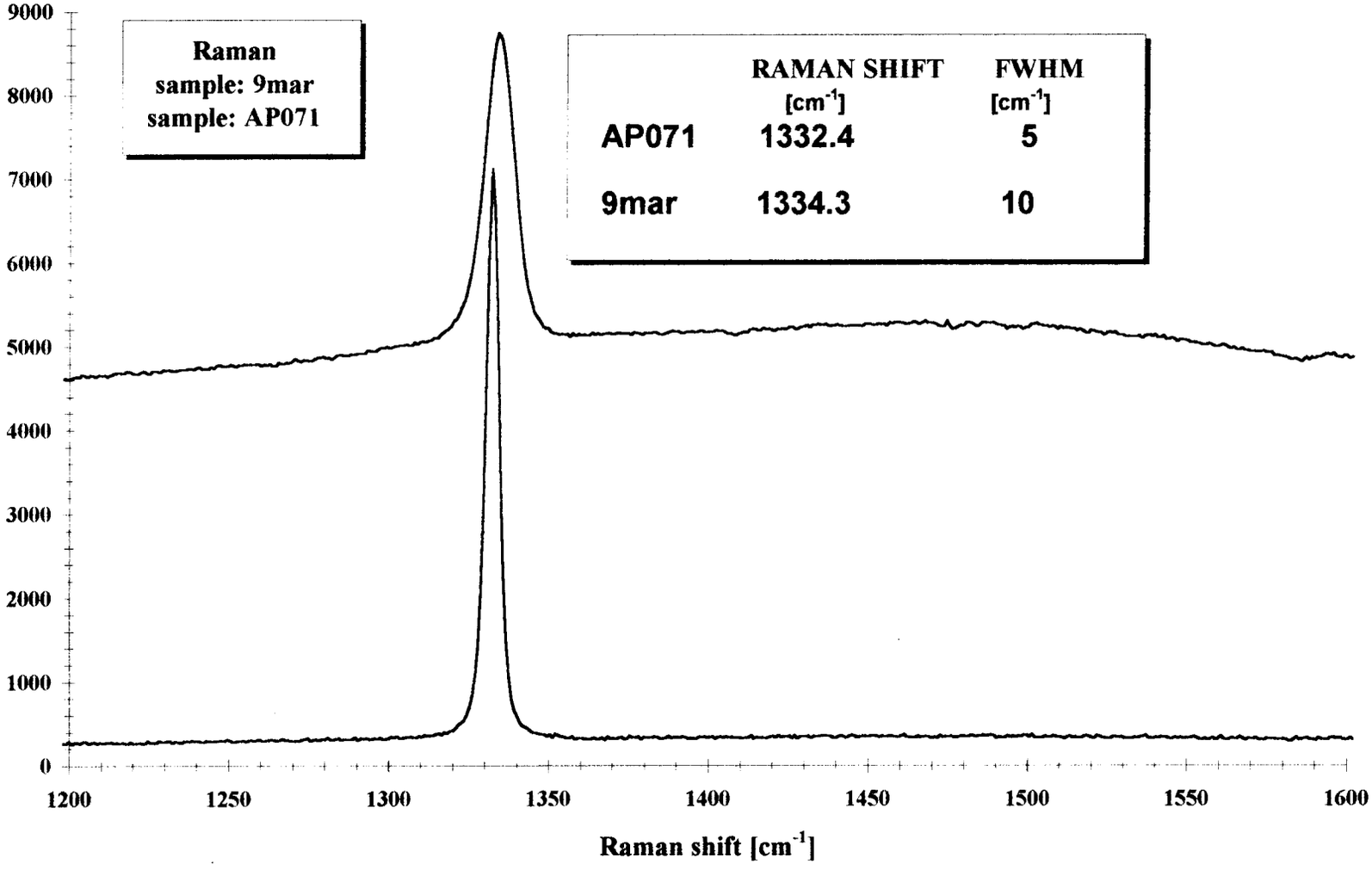
Raman
sample: 9mar
sample: AP071
RAMAN SHIFT [cm-1]
FWHM [cm-1]
AP071 1332.4 5
9mar 1334.3 10
9000
8000
7000
6000
5000
4000
3000
2000
1000
0
1200
1250
1300
1350
1400
1450
1500
1550
1600
Raman shift [cm-1]


01 µm 15.2kV 503E2 2112/95 AP071

a)


10 µm 15.2kV 298E3 2111/95 AP071

b)

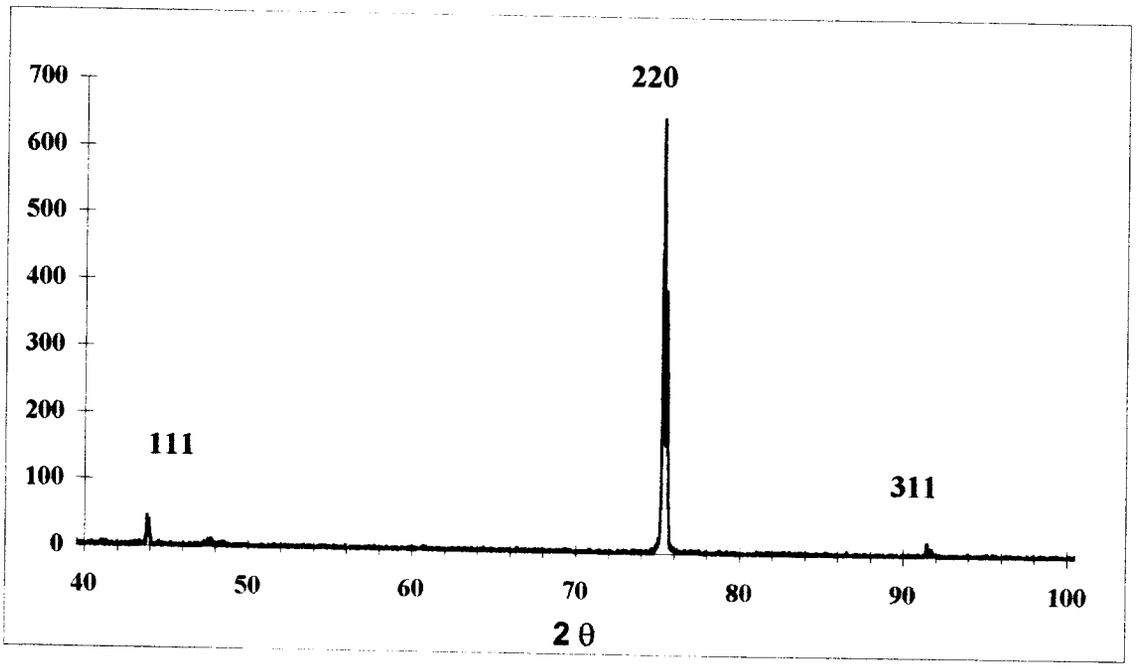
700
600
500
400
300
200
100
0
220
111
311
40
50
60
70
80
90
100
2 θ

a)

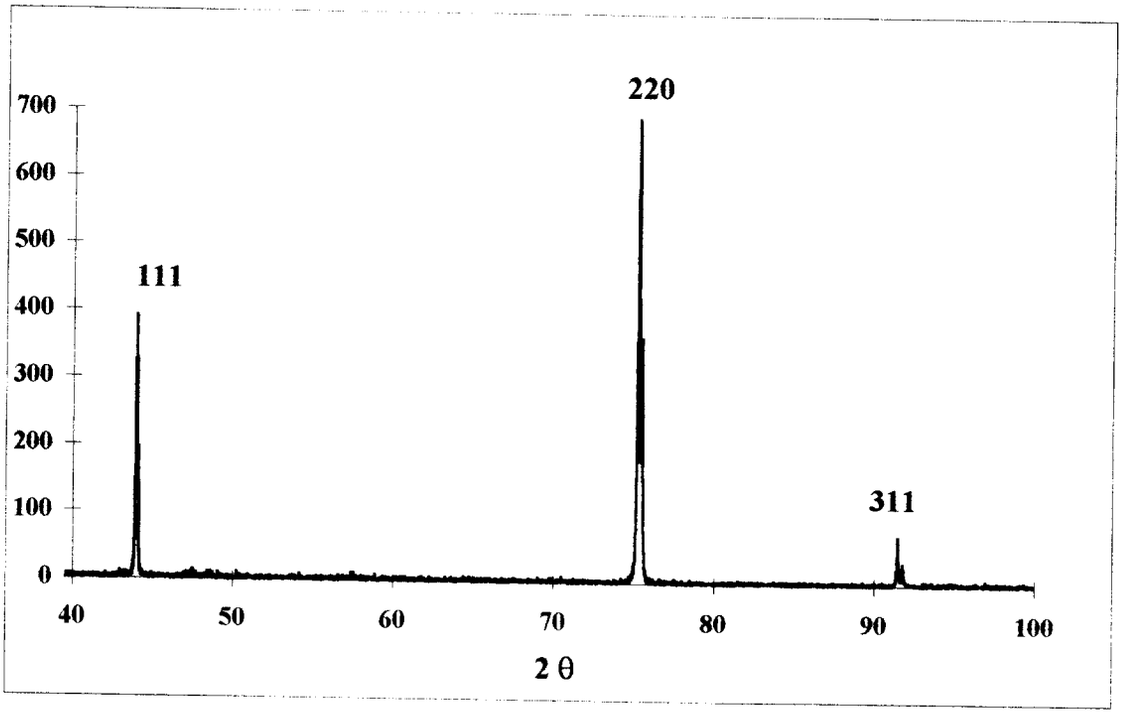
700
600
500
400
300
200
100
0
220
111
311
40
50
60
70
80
90
100
2 θ

b)

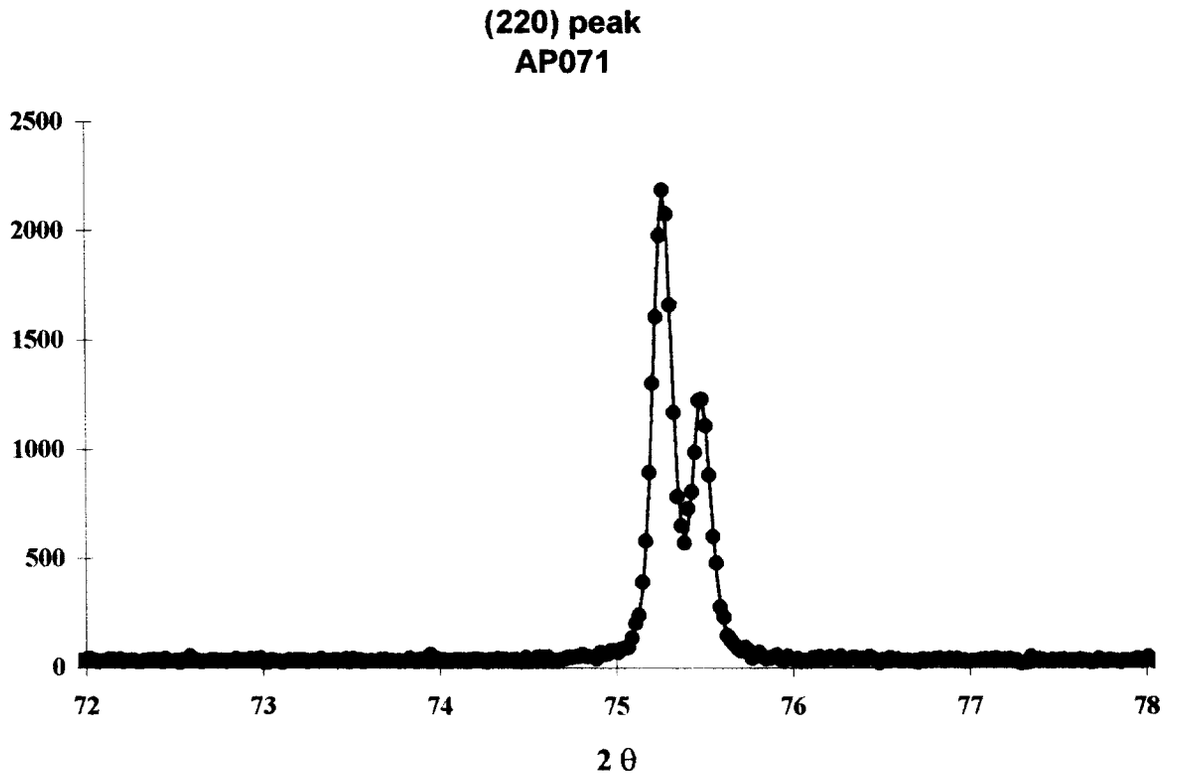
(220) peak
AP071
2500
2000
1500
1000
500
0
72
73
74
75
76
77
78
2 θ

a)

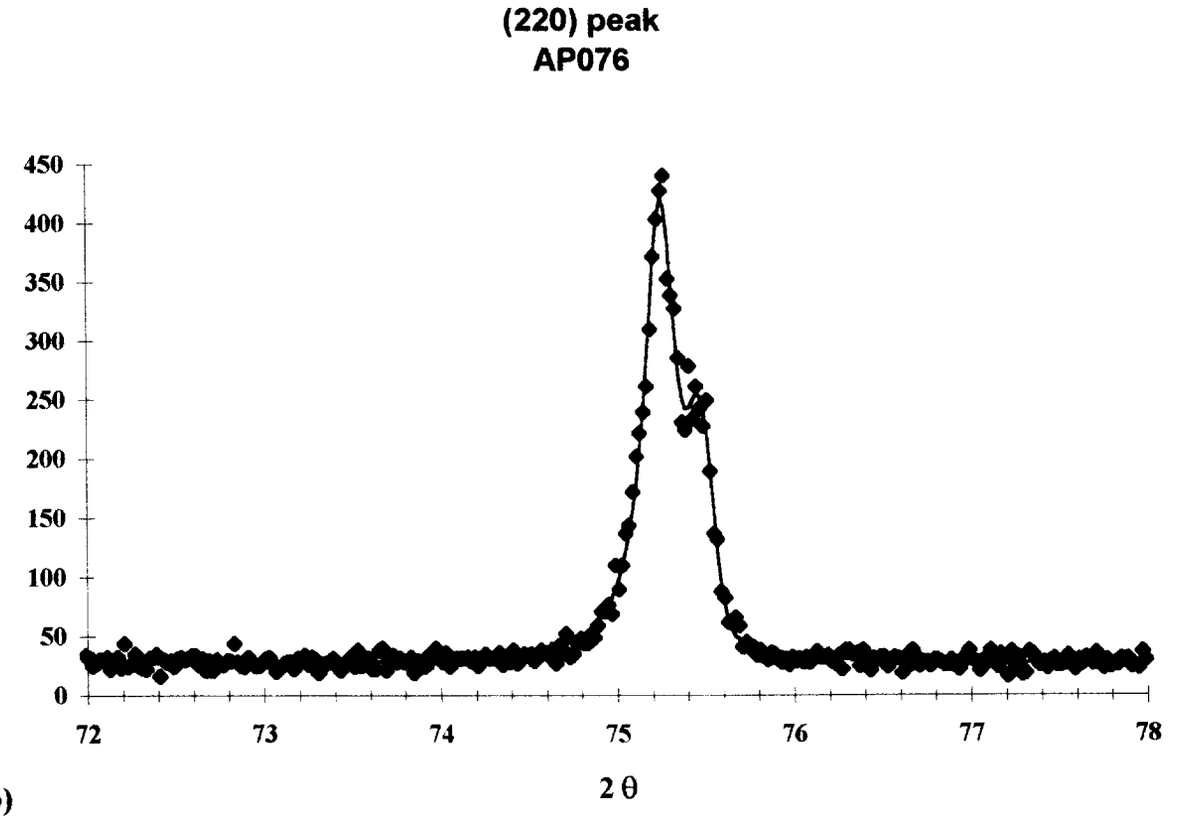
(220) peak
AP076
450
400
350
300
250
200
150
100
50
0
72
73
74
75
76
77
78
2 θ

b)

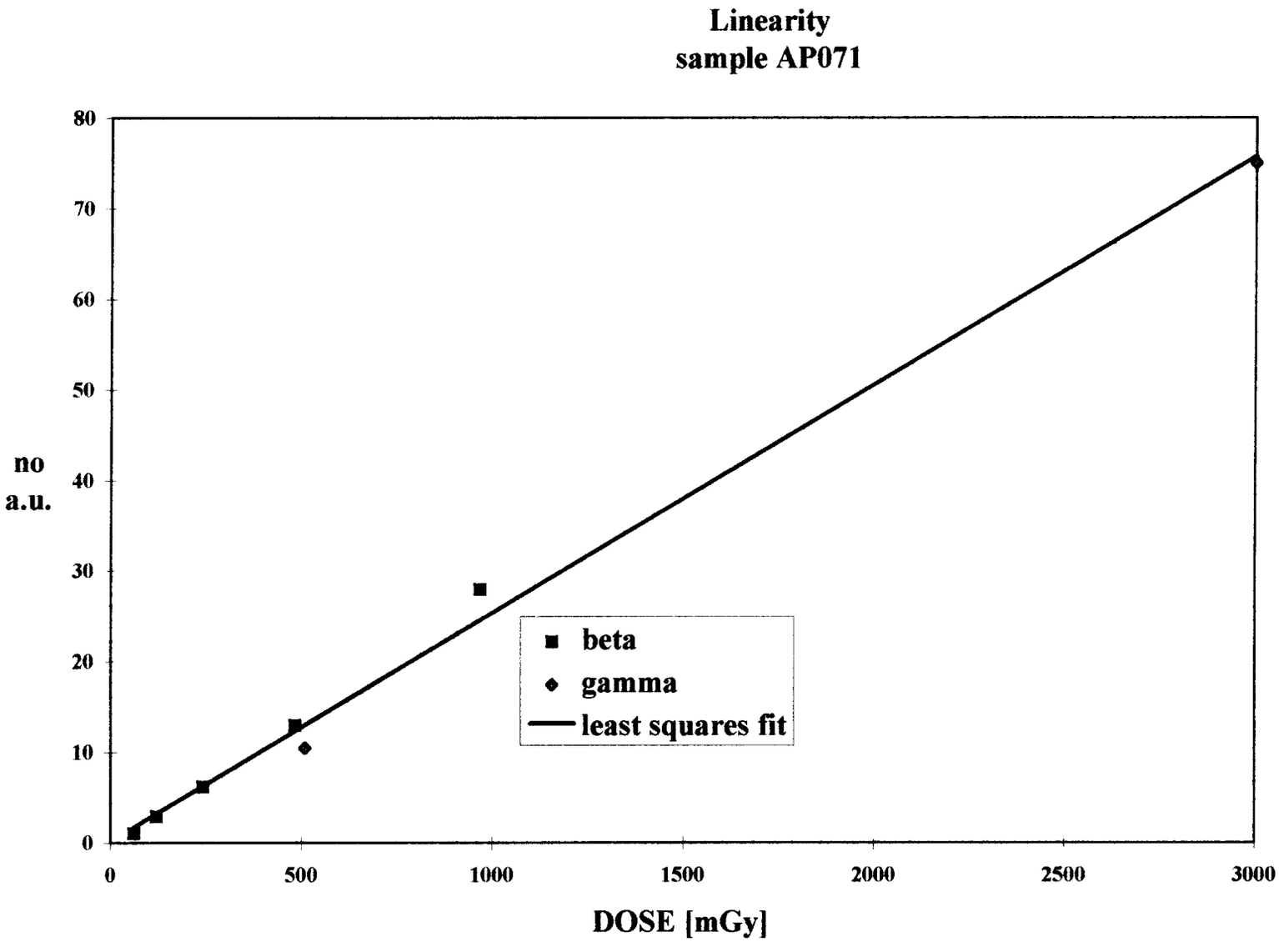
Linearity
sample AP071
no
a.u.
80
70
60
50
40
30
20
10
0
0
500
1000
1500
2000
2500
3000
DOSE [mGy]
beta
gamma
least squares fit

Linearity
sample AP076

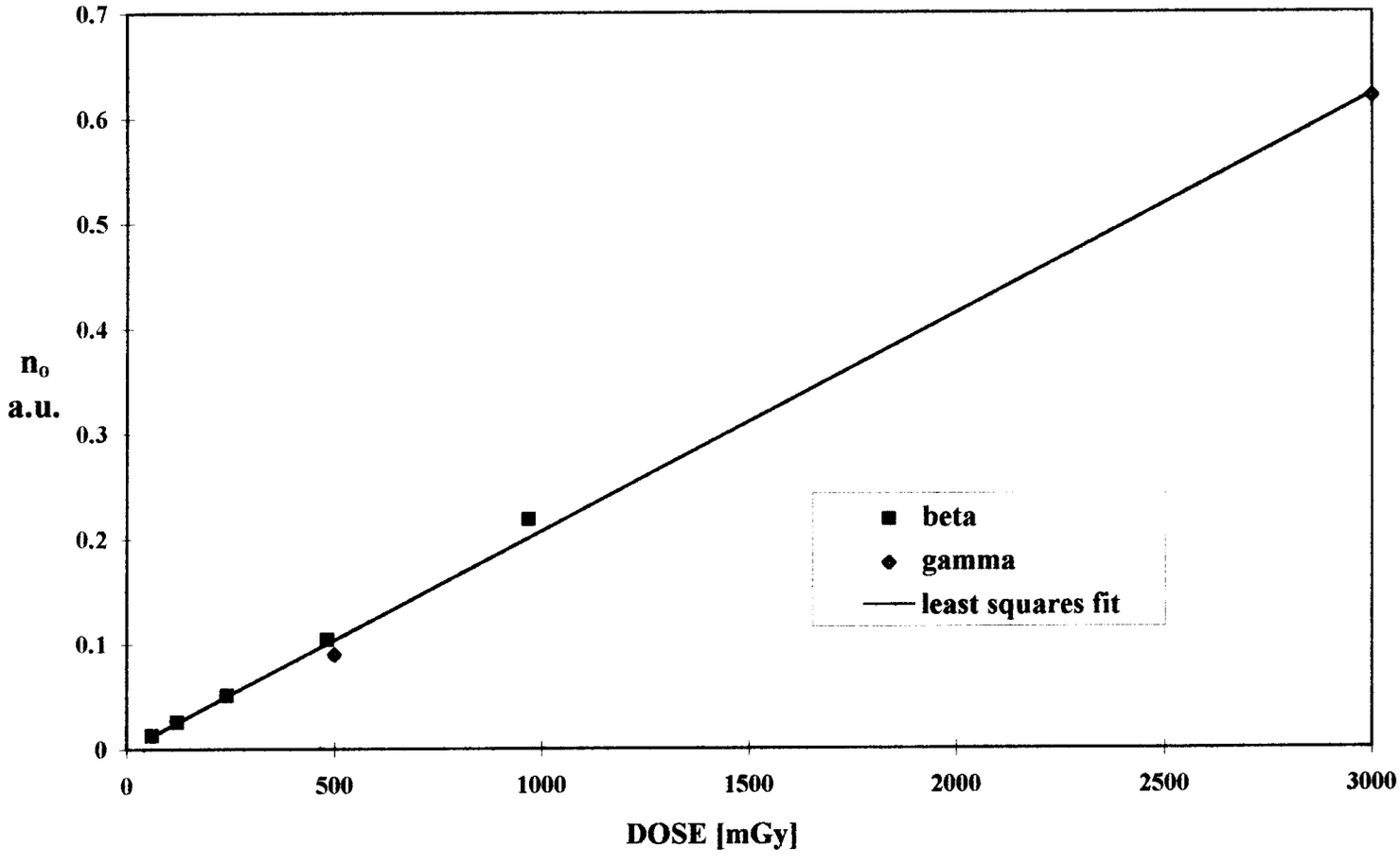

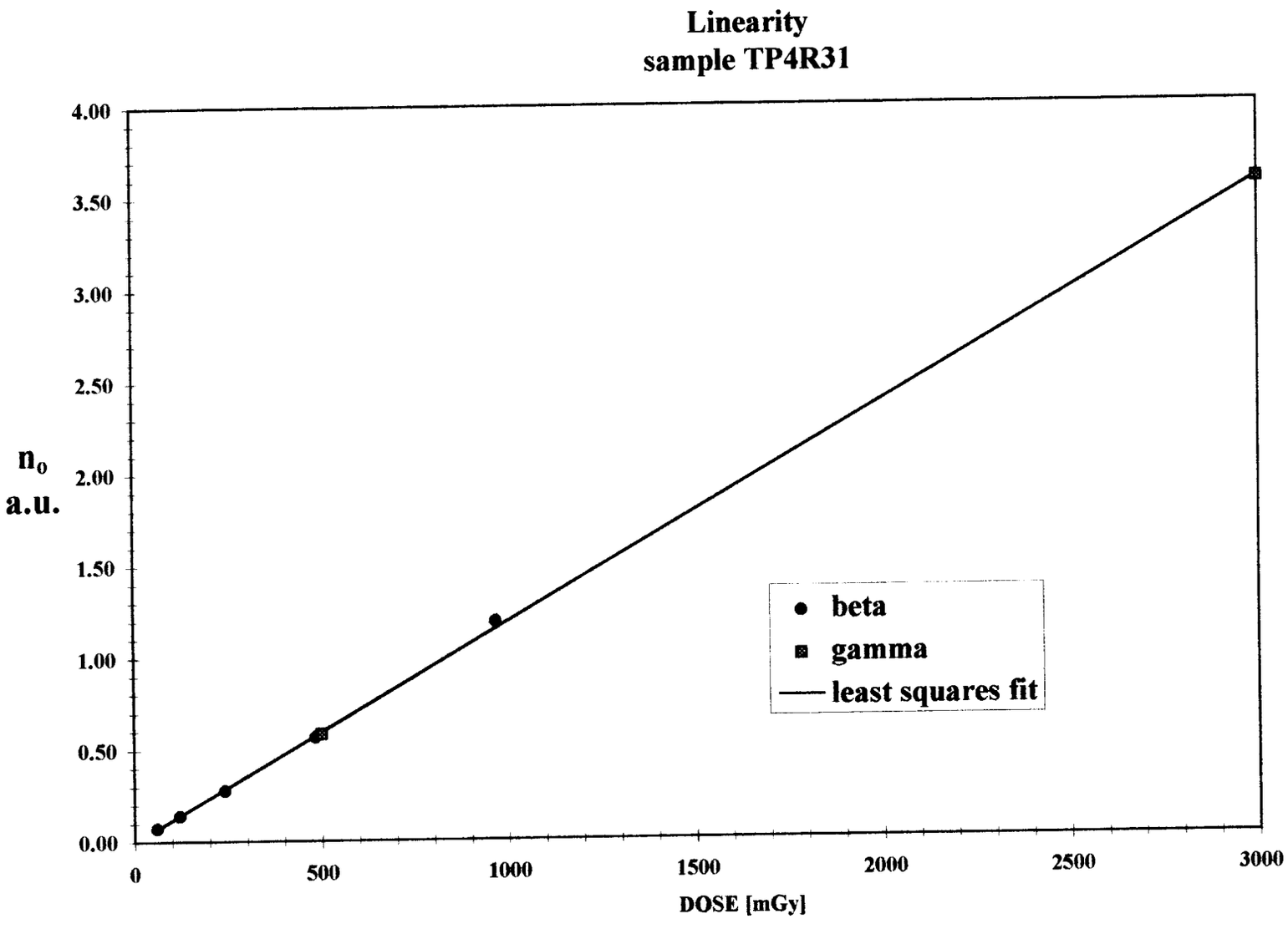
Linearity
sample TP4R31
4.00
3.50
3.00
2.50
2.00
1.50
1.00
0.50
0.00
n0
a.u.
0
500
1000
1500
2000
2500
3000
DOSE [mGy]
beta
gamma
least squares fit

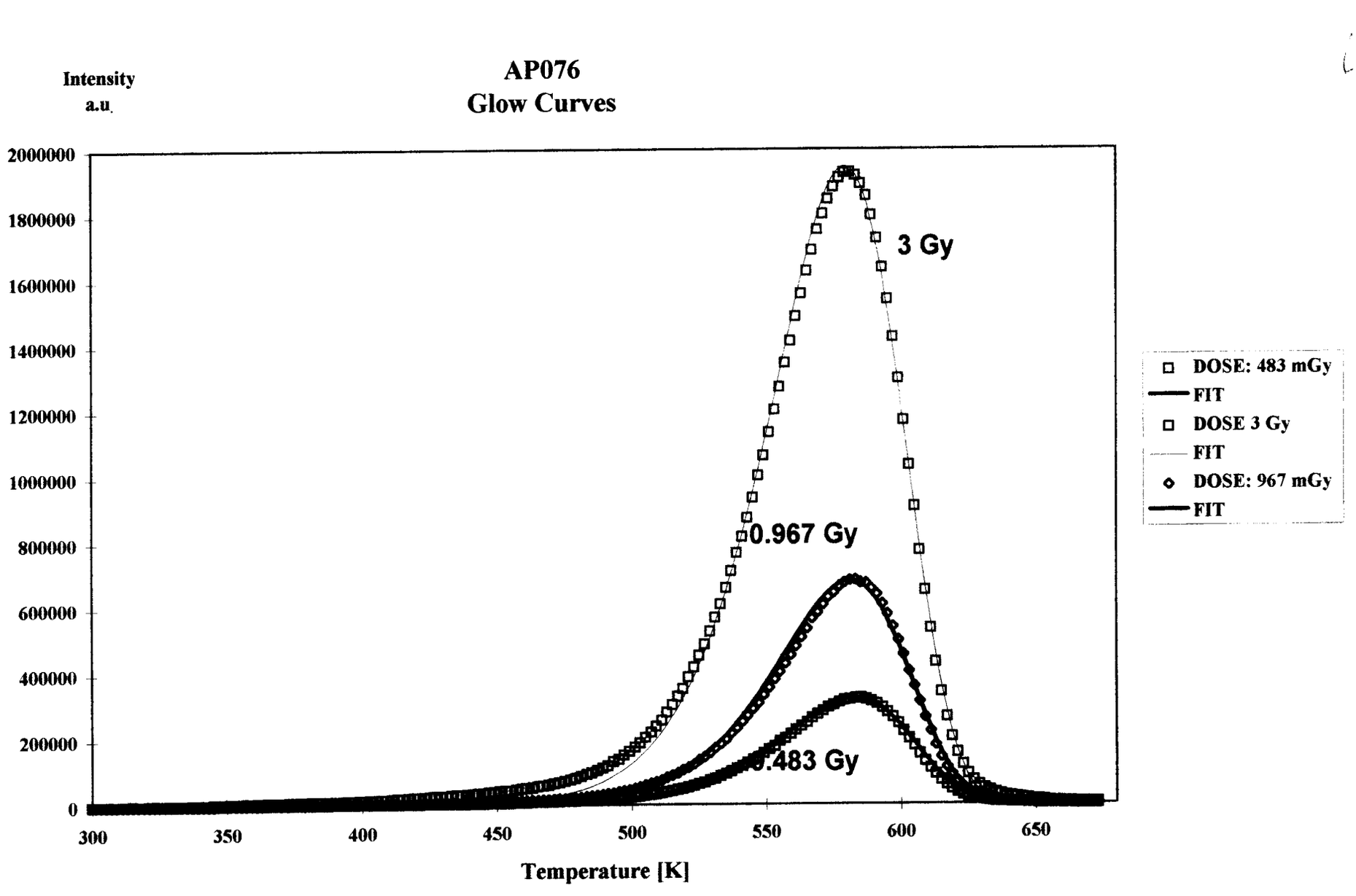
AP076
Glow Curves
Intensity
a.u.
2000000
1800000
1600000
1400000
1200000
1000000
800000
600000
400000
200000
0
300
350
400
450
500
550
600
650
Temperature [K]
3 Gy
0.967 Gy
.483 Gy
DOSE: 483 mGy
FIT
DOSE 3 Gy
FIT
DOSE: 967 mGy
FIT

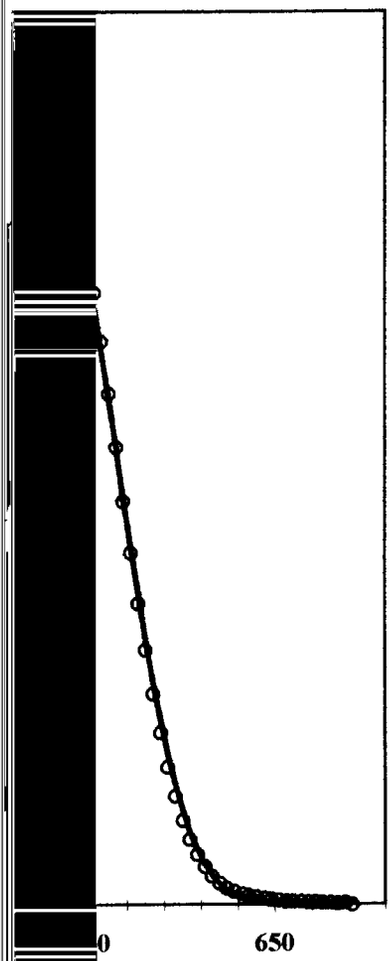
0
650

Glow curve
sample TP4R31
dose: 3Gy